Available online at www.sciencedirect.com
SCIENCE DIRECT®
Journal of Nuclear Materials 334 (2004) 28–34
journal of nuclear materials
www.elsevier.com/locate/jnucmat

Reactivity of hydrogen peroxide towards Fe_3O_4, Fe_2CoO_4 and Fe_2NiO_4

Maryam Abili Nejad, Mats Jonsson *

Department of Chemistry, Nuclear Chemistry, Royal Institute of Technology, SE-100 44 Stockholm, Sweden

Received 22 December 2003; accepted 22 April 2004

Abstract

The kinetics of CRUD oxidation by H_2O_2 has been studied using aqueous suspensions of metal oxide powder. Fe_3O_4, Fe_2CoO_4 and Fe_2NiO_4 were used as model compounds for CRUD. In addition, the activation energies for the reaction between H_2O_2 and the three CRUD models were determined. The rate constants at room temperature were determined to $6.6\ (\pm 0.4)\times 10^{-9}$, $3.4\ (\pm 0.4)\times 10^{-8}$ and 1.6×10^{-10} m min^{-1} for Fe_3O_4, Fe_2CoO_4 and Fe_2NiO_4, respectively. The corresponding activation energies are 52 ± 4, 44 ± 5 and 57 ± 7 kJ mol^{-1}, respectively. The mechanism of the reaction is briefly discussed indicating that the final solid product in all three cases is Fe_2O_3. In addition to the experimental studies, the theoretical grounds for kinetics of reactions in particle suspensions are discussed. The theoretical discussion is also used to explain the somewhat unexpected trends in reactivity observed experimentally.

PACS: 82.50.G

1. Introduction

Corrosion products formed in water-cooled nuclear reactors cause a wide range of problems due to transportation of radioactivity and deposition on heat exchanging surfaces. The corrosion products released from out-of-core metal surfaces are transported with the coolant to the core where they can deposit on fuel surfaces to build up fuel CRUD (Chalk River Unidentified Deposit, mostly containing Fe_2O_3, Fe_3O_4, Fe_2CoO_4, and Fe_2NiO_4) [1,2]. The corrosion products in the core are exposed to a high flux of neutrons and thereby become activated. In-core corrosion species may already be activated before they are released [3,4]. Radioactive CRUD could be released from fuel surfaces and is subsequently transported (by the coolant) to other parts of the systems where it can deposit on surfaces (e.g. pipework surfaces). Although, most of the corrosion products can be stopped by various filtration techniques [5] there is still a fraction of activated particles escaping into other parts of the coolant cycle. Power plant personnel may thus be exposed to increased levels of ionizing radiation.

Radiolysis of coolant water causes decomposition of water to radical and molecular products, including H_2O_2 [6]. Apart from the homogeneous radiation chemical reactions, radiolytically formed oxidants and reductants also react with solid metal oxides, e.g., CRUD and ZrO_2. Hence, reactions between radiolysis products and CRUD must be considered to understand reactor chemistry in general and the mechanism of CRUD formation and CRUD stability in particular.

To the best of our knowledge, there are only a few publications on the reaction between H_2O_2 and metal oxide materials at a mechanistic level. Ishigure et al. [4,7] investigated the effects of γ-radiation and H_2O_2 addition on the release of corrosion products in a reaction system consisting of aqueous solution of O_2 and stainless steel

* Corresponding author. Tel.: +46-8 790 9123; fax: +46-8 790 8772.
E-mail address: matsj@nuchem.kth.se (M. Jonsson).

0022-3115/$ - see front matter © 2004 Elsevier B.V. All rights reserved.
doi:10.1016/j.jnucmat.2004.04.325

at high temperature (250 °C). Their results clearly show that γ-radiation increases the oxide film thickness on stainless steel as well as the release of low solubility iron CRUD. Addition of H_2O_2 decreases the release of low solubility iron CRUD while there is no significant effect on the release of cobalt CRUD [8]. In a series of papers, Wada et al. studied the effect of H_2, O_2 and H_2O_2 on oxide film formation [9]. Kim bases his work on a detailed analysis of the surface oxidation of stainless steel immersed in aqueous solutions containing the above redox agents [10,11]. These studies provide some insights into the relative effects of H_2, O_2 and H_2O_2 on CRUD formation and stability. In the presence of H_2O_2, the main oxide formed is hematite (Fe_2O_3) while magnetite (Fe_3O_4) is the main oxide formed in the presence of O_2. The product pattern reflects the relative oxidant strength (i.e. the standard reduction potential) of the two oxidants. It was also found that iron chromate ($FeCr_2O_4$) structures are formed in the presence of O_2 while Cr-deficient/Ni-enriched magnetite structures are formed in the presence of H_2O_2. This indicates that oxidation of stainless steel by O_2 is thermodynamically controlled while oxidation by H_2O_2 is kinetically controlled (Ni is much more difficult to oxidize than is Cr). Decomposition of H_2O_2 over heterogeneous catalysts such as Ag, Cu, Fe, Mn, Ni, and Pt and their oxides has been previously investigated [12–18]. A detailed analysis of the decomposition of H_2O_2 on goethite (α-FeOOH) can be found in the work by Lin and Gurol [19]. They showed that the reaction between H_2O_2 and goethite follows a second order kinetic expression $-d[H_2O_2]/dt = k[\text{FeOOH}][H_2O_2]$. Decomposition of H_2O_2 under simulated BWR conditions in stainless steel or titanium tubing has been studied by Lin et al. [20]. The activation energy for H_2O_2 decomposition in stainless steel or titanium tubing was found to be 14.8 and 16.3 kcal mol^{-1} (61.9 and 68.2 kJ mol^{-1}), respectively. Based on the relatively low activation energies and the fact that no free hydroxyl radicals could be detected in the system, they argued that the mechanism for H_2O_2 decomposition is catalytic decomposition due to a charge transfer process, i.e., the primary step is surface oxidation. A detailed investigation of reactions of magnetite suspensions with one-electron reductants from radiolysis of aqueous solutions of propan-2-ol has been done by Buxton et al. [21]. They show that simple homogeneous kinetics is applicable although the reactions take place at the solid–liquid interface.

Recently, the kinetics for oxidation of UO_2 in aqueous suspension by H_2O_2 and some other oxidants was studied [22]. These reactions displayed first order kinetics with respect to oxidant concentration and with respect to surface/volume ratio, i.e., the total reaction order is 2. In addition, the logarithm of the second order rate constant was found to be linearly dependent on the one-electron reduction potential of the oxidant.

In this work, we have investigated the reactivity of H_2O_2, towards nickel and cobalt iron oxides and magnetite at various temperatures to allow extrapolation to reactor conditions. This investigation can help us to understand the mechanism of formation and stability of CRUD layers.

2. Experimental

The three metal oxides Fe_3O_4, Fe_2CoO_4 and Fe_2NiO_4 were purchased from KEBO and Alfa Aesar. The chemicals used throughout this study were of analytical grade or purer obtained from commercial sources as Aldrich, Merck, BDH and AGA. The water used was Millipore purified prior to use.

The concentration of hydrogen peroxide used in the experiments was approximately 5 mM. 0–10 g of solid metal oxide powder was added to the hydrogen peroxide solution to reach 20 ml suspension volume. The H_2O_2 solution was purged with Ar for 20 min prior to oxide addition and the suspension was purged throughout the experiment for mixing purposes and to keep the concentration of oxygen as low as possible. The solutions were protected from light throughout the experiments and subsequent analysis. Before each analysis, the solution was filtered to stop the reaction and to clear the solution (pore size 0.2 μm). The H_2O_2 concentration was then determined. Experiments were performed in the temperature range, 25–90 °C. Potassium iodide, KI, was used as indicator (according to the reactions: $H_2O_2 + 2H^+ + 2I^- \rightarrow 2H_2O + I_2$ and $I_2 + I^- \rightarrow I_3^-$) for analysis of the hydrogen peroxide concentration. The concentration of I_3^- was determined spectroscopically (using a Jasco V-530 UV–VIS) at 360 nm where I_3^- absorbs. The sensitivity of the method is quite high enabling measurement of micro-molar concentrations of H_2O_2.

The buffer solution used in this measurement contains 1 M of HAc, 1 M of NaAc, and a few drops of 3% ammoniumdimolybdate ($(NH_4)_2Mo_2O_7$) as a catalyst. The final solution contains 100 μl sample, 100 μl KI solution, 100 μl buffer solution and H_2O to reach a total volume of 2 ml [23–25].

The specific surface areas of the three metal oxides, Fe_3O_4, Fe_2CoO_4 and Fe_2NiO_4 powders were determined by BET measurement to be 6.59, 1.05 and 2.12 m^2 g^{-1}, respectively, using a Flowsorb 2300II at room temperature. The gas used in this method was a mixture of N_2 (30%) and He (70%).

Inductively coupled plasma (ICP) experiments were performed at room temperature with an inductively coupled plasma atomic emission (ICP-AES) model 3520 B instrument from Applied Research Laboratory. The uncertainty of the ICP-AES measurements is in the range 5–10%.

3. Result and discussion

A number of experiments were carried out to investigate the reaction of H_2O_2 with Fe_3O_4, Fe_2CoO_4 and Fe_2NiO_4. The H_2O_2 concentrations are plotted vs. reaction time in Fig. 1.

As can be seen, all three metal oxides appear to promote decomposition of H_2O_2. However, in these experiments the metal oxides were used as received, i.e., without prior purification. In these cases significant amounts of dissolved metal ions could be present. Hence, the decomposition of H_2O_2 could be strongly affected by homogeneous Fenton chemistry ($Fe^{2+} + H_2O_2 \rightarrow Fe^{3+} + OH^{\cdot} + OH^{-}$). To minimize the effect of soluble metal ions we repeated the experiments using metal oxides washed with EDTA and water. The results are shown in Fig. 2.

As can be seen, washing of the metal oxides significantly affects the dynamics of H_2O_2 decomposition. For all three metal oxides the rate of the reaction is significantly reduced. Interestingly, H_2O_2 is not decomposed to any detectable extent in the presence of Fe_2NiO_4 at room temperature (regardless of the amount of Fe_2NiO_4 used in the experiment) while both Fe_3O_4 and Fe_2CoO_4 facilitate decomposition. The reaction between H_2O_2 and Fe_2CoO_4 is close to first order with respect to H_2O_2 while the reaction between H_2O_2 and Fe_3O_4 displays autocatalytic behavior, i.e., the reaction rate increases with time. The latter can possibly be explained by slow release of Fe^{2+} giving rise to Fenton chemistry. As pointed out by the reviewer, the autocatalytic behavior could also be due to an increase of the accessible surface during the course of the reaction.

To analyze the inventory of soluble metal ions in the metal oxide powders used and to shed some light on the mechanism of the reaction between H_2O_2 and metal oxides we used ICP-AES (Inductively Coupled Plasma Atomic Emission). It should be noted that magnetite has thermodynamically a very high solubility at room temperature under reducing conditions and that it is not thermodynamically stable under oxidizing conditions. However, kinetic restrictions limit the actual solubility [26]. Three different types of samples were analyzed: (1) the metal oxides were mixed with distilled water and the aqueous phase (100 ml) was analyzed, (2) the metal oxides were mixed with an aqueous EDTA (0.1 M) solution and the solution (100 ml) was analyzed, (3) the metal oxides were washed with aqueous EDTA (0.1 M) solution and with pure water, filtered and thereafter added to an aqueous solution (20 ml) containing H_2O_2 (5 mM). The latter solution was analyzed after 20 min Ar-purging while the solutions in the former two experiments were in contact with the metal oxide powders for 30 min. In all three cases the amounts of Fe_3O_4, Fe_2CoO_4 and Fe_2NiO_4 were 0.5, 1.5 and 2 g, respectively, to obtain comparable surface to volume ratio. The solutions were filtered to remove the metal oxide powder prior to ICP-AES analysis. The results are given in Table 1.

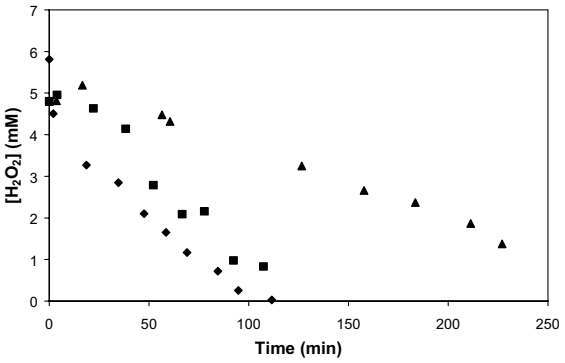

Fig. 1. H_2O_2 concentration as a function of reaction time at 25 °C, metal oxides were used as received: (◆) Fe_3O_4 1.2 g, (■) Fe_2CoO_4 3 g, (▲) Fe_2NiO_4 3 g.

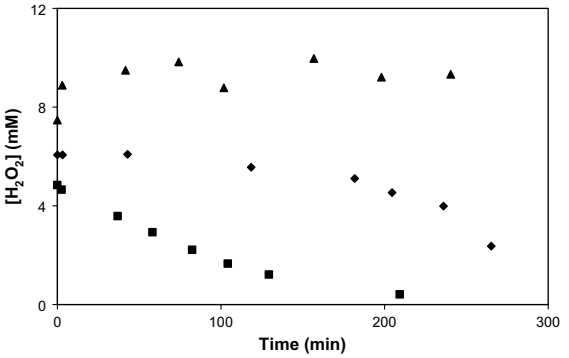

Fig. 2. H_2O_2 concentration as a function of reaction time, at 25 °C, metal oxides were pre-washed with EDTA 0.1 M and with distilled water: (◆) Fe_3O_4 0.5 g, (■) Fe_2CoO_4 1.5 g, (▲) Fe_2NiO_4 2 g.

The ICP-AES measurements on the aqueous phase (sample type 1) and EDTA solution (sample type 2) show that Fe_3O_4 contains considerable amounts of dissoluble iron. Considerable amounts of dissoluble cobalt and nickel are also found for Fe_2CoO_4 and Fe_2NiO_4, respectively. The dissoluble iron content in these oxides is also significant. Hence, the oxides must be washed with EDTA prior to the experiments in order to study the reaction between H_2O_2 and the metal oxide surfaces without significant disturbance from homogeneous Fenton chemistry. Qualitatively, it is also obvious that the reaction with H_2O_2 liberates additional metal ions from all three types of metal oxides (sample type 3). For Fe_2CoO_4 and Fe_2NiO_4 the major dissoluble products formed upon reaction with H_2O_2 are Co- and Ni-ions, respectively. For all three metal oxides the amount of dissoluble metal ions formed upon exposure to H_2O_2 (sample type 3) is significantly higher than what can be

Table 1
Metal ion concentrations measured by ICP at 25 °C

Sample	$[Fe^{3+/2+}]$ (M)	$[Co^{2+}]$ (M)	$[Ni^{2+}]$ (M)
Fe_3O_4[a]	2.3×10^{-6}	–	–
Fe_3O_4[b]	2.3×10^{-5}	–	–
Fe_3O_4[c]	7.7×10^{-5}	–	–
Fe_2CoO_4[a]	1.4×10^{-7}	1.6×10^{-5}	–
Fe_2CoO_4[b]	1.9×10^{-6}	3.3×10^{-5}	–
Fe_2CoO_4[c]	5.0×10^{-6}	5.2×10^{-5}	–
Fe_2NiO_4[a]	1.4×10^{-7}	–	0
Fe_2NiO_4[b]	4.5×10^{-6}	–	1.0×10^{-5}
Fe_2NiO_4[c]	1.8×10^{-5}	–	1.3×10^{-4}

[a] Metal oxides were mixed with distilled water and the aqueous phase (100 ml) was analyzed (exposure time 30 min).

[b] Metal oxides were mixed with an aqueous EDTA (0.1 M) solution (100 ml) and then the solution was analyzed (exposure time 30 min).

[c] Metal oxides were washed with aqueous EDTA (0.1 M) solution and thereafter added to an aqueous solution (20 ml) containing H_2O_2 (5 mM), then the final solution was analyzed.

extracted using the EDTA solution (sample type 2). This indicates that the finally formed solid is Fe_2O_3. Consequently, radiolytically produced H_2O_2 and probably also other oxidizing radiolysis products appear to be capable of transforming Fe_2MO_4-crud into Fe_2O_3-crud. This is well in line with previous studies reporting γ-Fe_2O_3 (maghemite) to be formed upon oxidation of Fe_3O_4 [27].

The simplest assumption concerning the reaction order for reactions between H_2O_2 and metal oxides is a second order reaction ($-d[H_2O_2]/dt = k[H_2O_2][MOX]$). However, under the conditions used in this work (excess of metal oxide) the reaction is expected to be of pseudo first order. To determine the second order rate constant for the reaction, the pseudo first order rate constant must be determined as a function of the amount of metal oxide. The second order rate constant is obtained from the slope of the linear plot of the pseudo first order rate constant against the amount of metal oxide (or more generally the surface to volume ratio) (Fig. 3). In Fig. 4 the concentration of H_2O_2 is plotted against the reaction time for three different amounts of Fe_3O_4.

As can be seen, the autocatalytic behavior observed for small amounts of Fe_3O_4 shifts to first order kinetics at higher surface to volume ratios. The resulting second order rate constants at room temperature for Fe_3O_4 and Fe_2CoO_4 are given in Table 2. Fe_2NiO_4 shows no reactivity at room temperature. The rate constant for Fe_2NiO_4 at room temperature was obtained from studies on the activation energy. It should be noted that all three metal oxides reduce MnO_4^- and $IrCl_6^{2-}$ at room temperature significantly faster than they reduce H_2O_2. The reaction with Fe_2NiO_4 is significantly slower than for the other metal oxides also when using these more

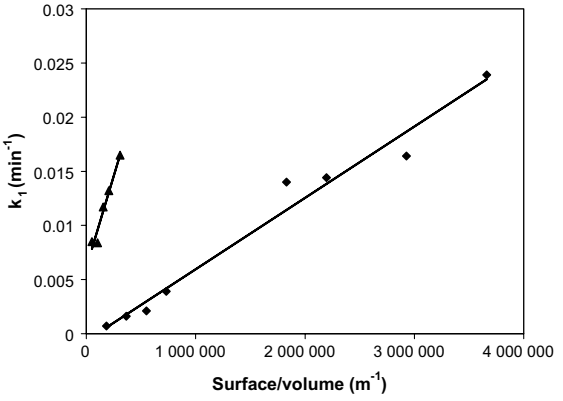

Fig. 3. Pseudo first order rate constants plotted against surface/volume ratio at 25 °C: (◆) Fe_3O_4, (▲) Fe_2CoO_4.

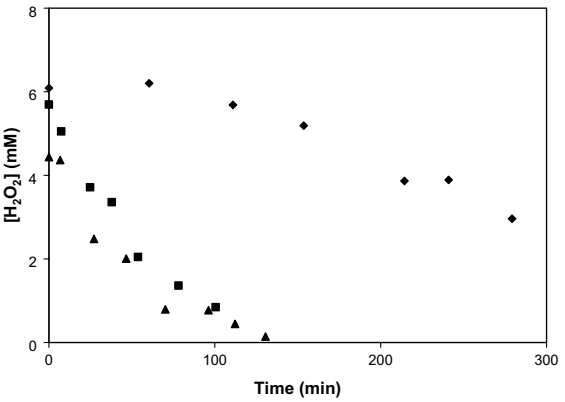

Fig. 4. H_2O_2 concentration as a function of reaction time for different amounts of magnetite (pre-washed with 0.1 M of EDTA and water) at 25 °C: (◆) 1.5 g, (■) 6 g, (▲) 10 g.

Table 2
Rate constants for reaction between metal oxides and hydrogen peroxide

Metal oxide	$k_{298(exp)}$ ($m\,min^{-1}$)	$k_{298(est)}$ ($min^{-1}\,m^{-1}$)[a]	$k_{573(est)}$ ($min^{-1}\,m^{-1}$)[a]
Fe_3O_4	$6.6\ (\pm0.4)\times10^{-9}$	2.7×10^{-8}	6.7×10^{-4}
Fe_2CoO_4	$3.4\ (\pm0.4)\times10^{-8}$	1.2×10^{-7}	6.4×10^{-4}
Fe_2NiO_4	–	1.6×10^{-10}	9.3×10^{-5}
UO_2	8.05×10^{-7}	–	–

[a] Estimated from Arrhenius parameters given in Table 3.

potent oxidants [28]. We also tested the reactivity of H_2O_2 towards α-Fe_2O_3 (hematite) at room temperature. However, no reaction was detected in this system even for very high amounts of hematite. For comparison, the rate constant for the reaction between H_2O_2 and UO_2 is also given in the table.

The trend in reactivity for the three metal oxides studied in this work is somewhat unexpected. From the

ionization potentials of the divalent metals in the oxides we would expect Fe to be more reactive than Co which in turn should be more reactive than Ni. For Fe and Co the observed trend is the reverse. However, the reaction between H_2O_2 and UO_2 is significantly faster than for any of the metal oxides studied here which is fully consistent with the expected thermodynamics of the process.

When studying the kinetics of heterogeneous systems the results cannot simply be analyzed as above, i.e., by only taking the solid surface area to solution volume into account. This approach is acceptable when comparing the reactivity of different solutes towards a given solid substrate as was done for UO_2-powder in Ref. [22]. However, when comparing the reactivity of different solid substrates towards a given solute (as in this work) we must base our comparison on the size of the solid particles in suspension. The theory behind this is relatively straight forward and has been described in detail by Astumian and Schelly [29]. In short, the rate constant is given by the Arrhenius equation (Eq. (1)):

$$k = A\mathrm{e}^{-\frac{E_a}{RT}}, \tag{1}$$

where A is the pre-exponential factor and E_a is the activation energy. If the activation energy is close to zero, the reaction is diffusion controlled and the rate constant is equal to the pre-exponential factor. Hence, the pre-exponential factor for a given reaction is identical to the diffusion controlled rate constant. The rate constant for a diffusion controlled bimolecular reaction is given by the following expression (Eq. (2)):

$$k_{\mathrm{diff}} = 4\pi N_A (D_1 + D_2) R_{12} f, \tag{2}$$

where N_A is the Avogadro constant, D_1 and D_2 are the diffusion coefficients of reactant 1 and 2, respectively, R_{12} is the collision distance $(R_1 + R_2)$ and f is an electrostatic factor depending on the charge of the reactants. If at least one of the reactants is uncharged, $f = 1$. Eq. (2) can also be expressed as Eq. (3) (using the Stokes–Einstein relationship); $D_x = RT/(N_A \pi \eta R_x)$ which describes the diffusion controlled kinetics in a homogeneous system (solution),

$$k_{\mathrm{diff}} = \frac{2k_B T}{3\eta} \frac{(R_1 + R_2)^2}{R_1 R_2}. \tag{3}$$

In Eq. (3), k_B denotes the Boltzmann constant and η is the viscosity of the solvent.

For heterogeneous systems we must consider the number of molecules on the surface of the particles being exposed to the solution. If reactant 1 is the solid material, Eq. (3) can then be written as (Eq. (4)):

$$k_{\mathrm{diff}} = \frac{2k_B T}{3\pi\eta} \frac{R_1^2}{R_2 R_p}, \tag{4}$$

where R_p is the particle radius and R_1 is the molecular radius of component 1 (e.g. Fe_2MO_4). The complete rate expression in the system under study in this work is given by Eq. (5).

$$\frac{\mathrm{d}[H_2O_2]}{\mathrm{d}t} = -\frac{2k_B T}{3\pi\eta} \frac{R_{\mathrm{MOX}}^2}{R_{H_2O_2} R_p} \left(\mathrm{e}^{-\frac{E_a}{RT}}\right) [H_2O_2] \frac{N_{\mathrm{MOX}}}{V}, \tag{5}$$

N_{MOX} denotes the amount of metal oxide molecules on the surface of the particles being exposed to the solution of volume V. The N_{MOX}/V ratio is proportional to the solid surface area to solution volume ratio used when deriving the second order rate constants.

To be able to compare the reactivity of H_2O_2 towards the different metal oxide powders we must normalize the experimentally determined rate constants to the same particle size. The approximate particle radii for the three metal oxides used in this work are 91, 571 and 283 μm for Fe_3O_4, Fe_2CoO_4 and Fe_2NiO_4, respectively. For comparison, the particle radius for the UO_2-powder used in Ref. [22] is 47 μm. The approximate particle radii were estimated from the specific surface area (determined by BET) and the density of the materials. It should also be noted that the particles of a given powder are not uniform in size. The estimated particle radii are merely describing the average size. To correctly perform the following comparison we would need to account for the particle size distribution. However, using the average particle radii is acceptable for a qualitative comparison. Assuming R_{MOX} to be identical for all three metal oxides we obtain the following relative k_{diff} for Fe_3O_4, Fe_2CoO_4 and Fe_2NiO_4, respectively: 1/0.16/0.32. However, since the reactions are far from being diffusion controlled, we also need the activation energies to be able to make the comparison. This was accomplished by measuring the rate constants for the reactions between H_2O_2 and the three metal oxides in the temperature range 25–90 °C. The Arrhenius plot for Fe_2CoO_4 is presented in Fig. 5 and the resulting activation energies and pre-exponential factors are given in Table 3.

It should be noted that the Arrhenius parameters were determined from the pseudo first order rate constants (i.e., the amount of metal oxide was not varied). This does not affect the activation energy. However, to obtain the correct pre-exponential factor the ratio between the pseudo first order rate constants and the solid surface area to solution volume ratio of the system were used for the Arrhenius plot. Interestingly, the relative relation between the three pre-exponential factors is virtually identical to the relation obtained from Eq. (5) and the approximate particle sizes.

As can be seen in Table 3, the trend in activation energy qualitatively parallels the trend for the reactivity of the three metal oxides towards H_2O_2 at room temperature. The activation energies reported in Table 3 are

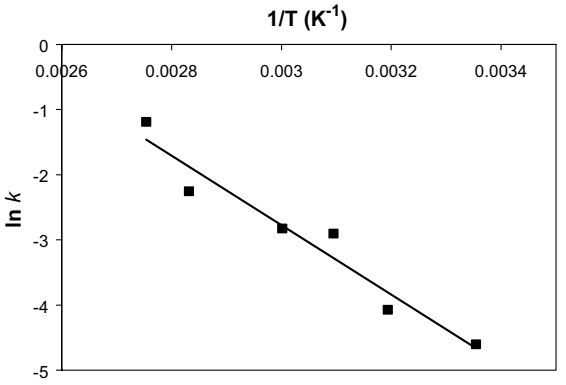

Fig. 5. $\ln k$ plotted against $1/T$ for Fe_2CoO_4.

Table 3
Arrhenius parameters

Metal oxide	$\ln A$	E_a (kJ mol^{-1})
Fe_3O_4	3.7	52 ± 4
Fe_2CoO_4	2.0	44 ± 5
Fe_2NiO_4	2.6	57 ± 7

somewhat lower than the activation energies reported for decomposition of H_2O_2 under simulated BWR conditions in stainless steel or titanium tubing (61.9 and 68.2 kJ mol^{-1}) [20]. As pointed out before, this trend is quite unexpected from a thermodynamical point of view. However, it should be noted that the particle size might also affect the activation energy of the process. The physicochemical properties of nanometer size particles are known to differ significantly from those of molecules and bulk materials [30]. Previously published results on H_2O_2 oxidation of UO_2 as a function of particle size can be employed to shed some light on the effect of particle size. In Ref. [31], the initial dissolution rates for UO_2 suspended in 0.01 m H_2O_2 were 7.05×10^{-11}, 9.00×10^{-11} and 9.24×10^{-11} (mol s^{-1} m^{-2}) for 900–1100 μm particles, a fuel pellet and 10–50 μm particles, respectively. It has been shown that the initial rate of dissolution is proportional to the rate of oxidation [22]. Using Eq. (4) we can calculate the relative values for k_{diff} and consequently the relative pre-exponential factors to 0.025, 0.0025 and 1, respectively. Since the rates are normalized to the surface exposed to the solution and the initial H_2O_2 concentration is the same in all three systems, the observed dissolution rates are directly proportional to the rate constants. Hence, we can use the published rates and the calculated relative pre-exponential factors to estimate the relative activation energies for the three different particle sizes according to the Arrhenius equation. The resulting relative activation energies are plotted against the particle size in Fig. 6.

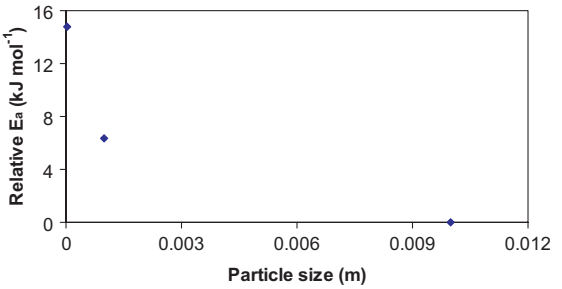

Fig. 6. The relative activation energy for $H_2O_2 + UO_2$ as a function of particle size.

From this example it is obvious that the particle size also affects the activation energy and that even mm-sized particles have considerably higher activation energies than the bulk material. We speculate that this can be attributed to the simple fact that larger particles contain more electrons than smaller particles. Hence, the barrier for removal of electrons (per m^2) from the particle should decrease with increasing electron content since the number of surface sites increases with r^2 while the number of electrons increases with r^3. A simple approach would then be to describe the activation energy based on the Boltzmann distribution (Eq. (6))

$$\frac{n_s}{n_b} = e^{-\frac{E_{a(s)}-E_{a(b)}}{k_B T}}, \tag{6}$$

where n_s and n_b are the number of molecules on the surface and in the bulk of the particle, respectively. The difference in activation energy between a particle of a given size and the corresponding bulk material is then given by Eq. (7).

$$-\Delta E_a = k_B T \ln \frac{n_s}{n_b}. \tag{7}$$

Hence, the deviation in activation energy for a particle compared to the bulk material should be proportional to the logarithm of the particle radius (since n_s is proportional to the particle surface area and n_b is proportional to the particle volume). In Fig. 7 we have plotted the relative activation energy against $\ln r$ for the UO_2 system described above.

As can be seen, the assumption appears to be reasonable based on the limited set of data available. Similar observations have recently been made for other heterogeneous systems [32,33].

In general, Eq. (7) can be used to normalize the activation energies. However, for the three metal oxides studied in this work the experimental uncertainty is too large. Hence, normalizing the experimental results obtained in this work to reactor conditions would be too speculative. Moreover, a comparison to the results on

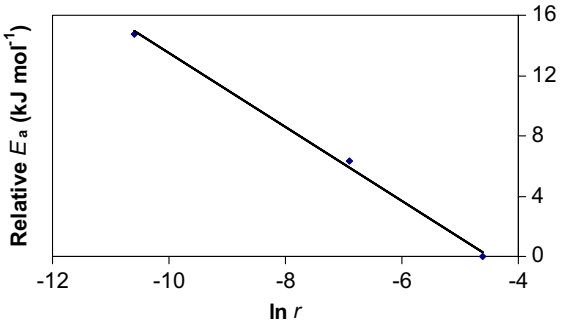

Fig. 7. The relative activation energy for $H_2O_2 + UO_2$ as a function of $\ln r$.

decomposition of H_2O_2 under simulated BWR conditions in stainless steel or titanium tubing are not justified due to the geometrical differences in the materials used.

4. Conclusions

In this paper we have shown that H_2O_2 reacts with the CRUD model compounds Fe_3O_4, Fe_2CoO_4 and Fe_2NiO_4. At room temperature no reactivity towards Fe_2NiO_4 is observed. However, at elevated temperatures the reactivity towards all three metal oxides is significant. The experiments indicate that the final solid product in all three cases is Fe_2O_3. The trend in reactivity is somewhat unexpected ($Fe_2CoO_4 > Fe_3O_4 > Fe_2NiO_4$) but can probably be attributed to the difference in particle size between the three metal oxides. It is also shown that the pre-exponential factor as well as the activation energy strongly depends on the particle size. Consequently, comparison of kinetic data for particle suspensions should be treated carefully taking the particle size into account.

References

[1] Y. Nishino, T. Sawa, K. Ohsumi, H. Itoh, J. Nucl. Sci. Tech. 26 (1989) 1121.
[2] T. Marchl, G.U. Gerger, Water Chem. Reactor Syst. 5 (2) (1989) 13.
[3] M. Hoshi, E. Tachikawa, T. Suwa, C. Sagawa, C. Yonezawa, M. Tomita, M. Shimizu, K. Yamamoto, J. Nucl. Sci. Tech. 23 (1986) 612.
[4] K. Ishigure, M. Kawaguchi, K. Oshoma, N. Fujita, Water Chemistry of Nuclear Reactor Systems 2, Proc. Inter. Conf. (1981) 293.
[5] H.P. Hermansson, G. Persson, A. Reinvall, Nucl. Tech. 103 (1993) 101.
[6] B. Pastina, J. Isabey, B. Hickel, J. Nucl. Mater. 264 (1999) 309.
[7] K. Ishigure, Chem. Nucl. Reactor Syst. 5 (2) (1989) 91.
[8] K Isigure, M. Kawaguchi, K. Oshoma, N. Ftjita, Water chemistry II, BENS, paper 43, (1980).
[9] Y. Wada, A. Watanabe, M. Tachibana, K. Ishida, N. Uetake, S. Uchida, K. Akamine, M. Sambongi, Sh. Suzuki, K. Ishigure, J. Nucl. Sci. Tech. 38 (2001) 183.
[10] Y.J. Kim, Corrosion 55 (1999) 81.
[11] Y.J. Kim, Corrosion 51 (1995) 849.
[12] J. Weiss, Trans. Faraday Soc. 31 (1935) 1547.
[13] J. Weiss, Adv. Catal. 4 (1952) 343.
[14] C.B.J. Roy, Catalysis 12 (1968) 129.
[15] Y. Ono, N. Matsumura, N. Kitajima, S.I. Fukuzumi, J. Phys. Chem. 81 (1977) 1307.
[16] N. Kitajima, S.I. Fukuzumi, Y. Ono, J. Phys. Chem. 82 (1978) 1505.
[17] D.W. Mckee, J. Catal. 14 (1969) 355.
[18] J. Abbot, D.G. Brown, Int. J. Chem. Kinet. 22 (1990) 963.
[19] S.S. Lin, M.D. Gurol, Environ. Sci. Tech. 32 (1998) 1417.
[20] C.C. Lin, F.R. Smith, N. Ichikawa, T. Baba, M. Itow, Int. J. Chem. Kinet. 23 (1991) 971.
[21] G.V. Buxton, T. Rhodes, R.M. Sellers Soc, J. Chem. Faraday Trans. 79 (1983) 2961.
[22] E. Ekeroth, M. Jonsson, J. Nucl. Mater. 322 (2003) 242.
[23] T.C.J. Ovenston, W.T. Rees, Analyst 75 (1950) 204.
[24] Y. Nimura, K. Itagaki, K. Nanba, Nippon Suisan Gakk. 58 (1992) 1129.
[25] W.A. Patrick, H.B. Wanger, Analy. Chem. 21 (1949) 127.
[26] R.M. Cornell, U. Schwertmann, The Iron Oxides (1996).
[27] K.J. Gallagher, W. Feitknecht, U. Mannweiler, Nature 217 (1968) 1118.
[28] M. Abili Nejad, M. Jonsson, submitted to J. Nucl. Mater.
[29] R.D. Astumian, Z.A. Schelly, J. Am. Chem. Soc. 106 (1984) 304.
[30] G. Schmid, Clusters and Colloids, VCH, Weinheim, 1994.
[31] J. Gimenez, E. Baraj, M.E. Torrero, I. Casas, J. de Pablo, J. Nucl. Mater. 238 (1996) 64.
[32] R.K. Sharma, P. Sharma, A. Marita, J. Colloid Interface Sci. 265 (2003) 134.
[33] W. Suwanwatana, S. Yarlagadda, J.W. Gillespie Jr., J. Mater. Sci. 38 (2003) 565.